MOF-Derived Untrafine MnO Nanocrystals Embedded in Porous Carbon Matrix as High-Performance Anodes for Lithium-Ion Batteries

Fangcai Zheng, [a] Guoliang Xia,[a] Guoliang Xia, [a] and Qianwang Chen[a,b*]

[a]Hefei National Laboratory for Physical Science at Microscale, Department of Materials Science & Engineering & Collaborative Innovation Center of Suzhou Nano Science and Technology, University of Science and Technology of China, Hefei 230026, China

[b]High Magnetic Field Laboratory, Hefei Institute of Physical Science, Chinese Academy of Science, Hefei 230031, China
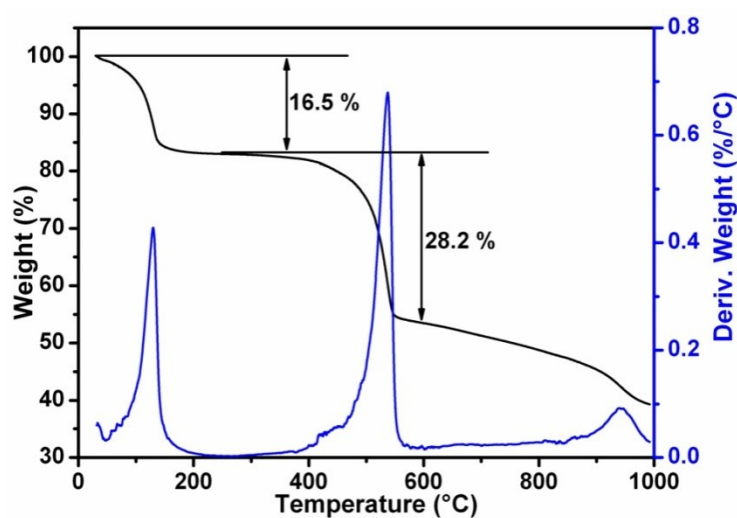
Figure S1. TGA curves of the Mn-BTC nanorods.

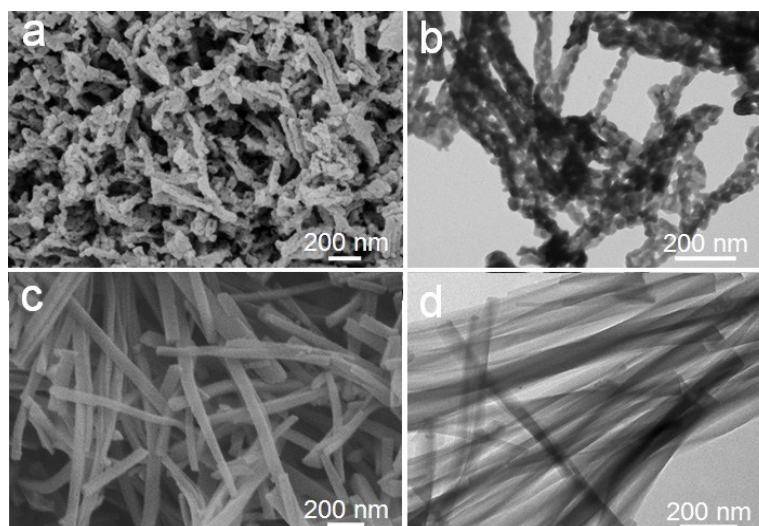* E-mail: cqw@ustc.edu.cn. Fax and Tel: +86 551 63603005.

Figure S2. SEM (a) and TEM (b) images of Mn$_2$O$_3$ through calcination of Mn-BTC in air; SEM (c) and TEM (d) images of pure C from MnO@C obtained at 570 °C.
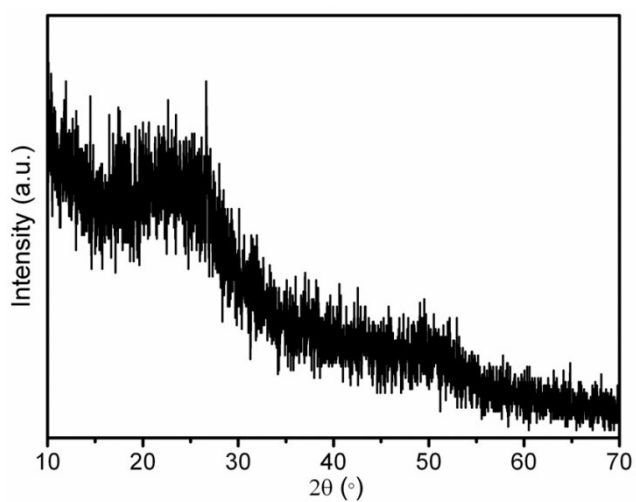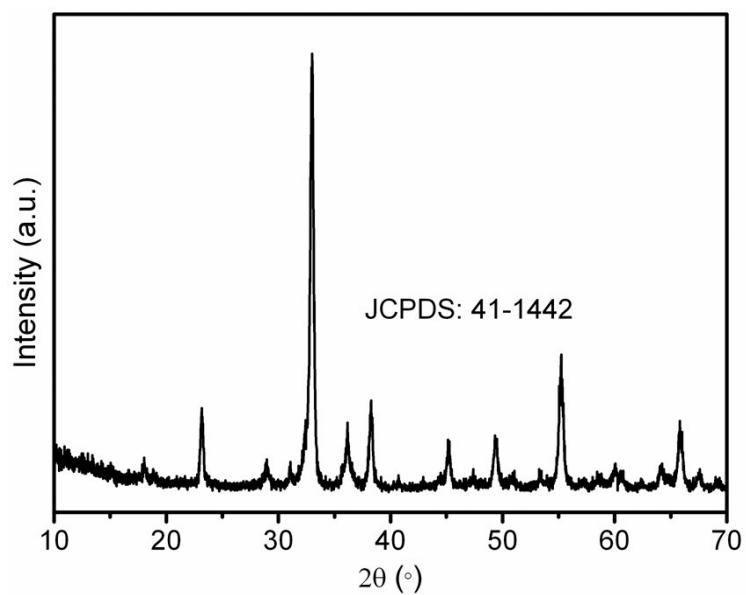

Figure S3. XRD pattern of pure C.
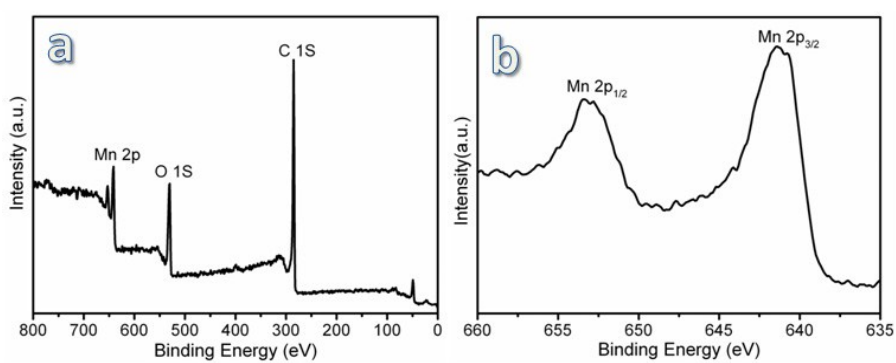
Figure S4. XRD pattern for Mn_2O_3.

Figure S5. (a) Survey XPS spectrum for the MnO@C nanorods and (b) high-resolution XPSspectrum for Mn 2p.
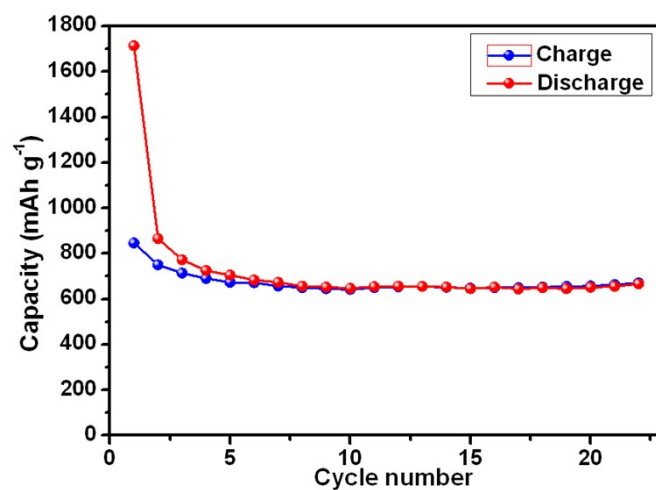
Figure S6. Cycle-life performance of MnO@C nanorods with the weight ratio of active material, acetylene black, and acetylene black as 8:1:1.
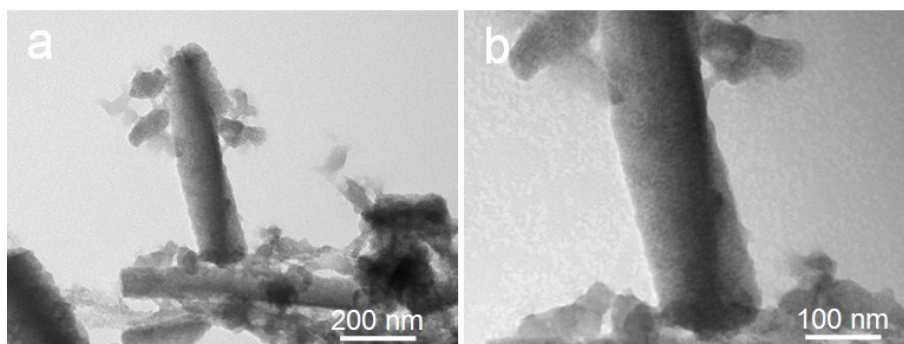

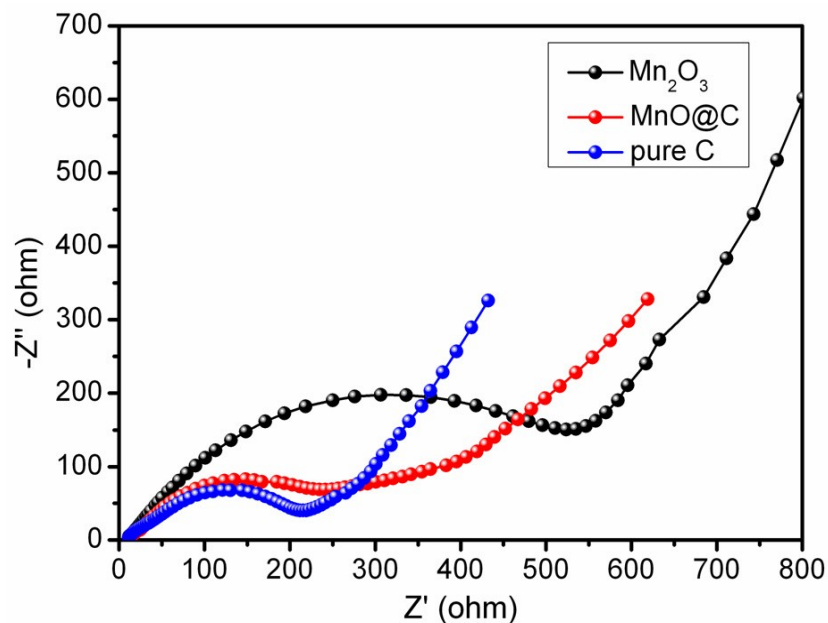**Figure S7.** TEM images of 620T-10R after 50 cycles (b) at a current density of 100 mA g^{-1}.

Figure S8. Impedance spectra of MnO@C, Mn_2O_3 and pure C, respectively.

Table S1. Comparison of BET specific surface area of various MnO/C hybrid anode materials

Samples	BET specific surface area ($m^2 g^{-1}$)	Reference
porous MnO/C microspheres	76.9	24
MnO/graphene	50.3	16
MnO@1-D carbon	64	45
Porous MnO/C nanotubes	40	17
MnO/C mesoporous networks	82.7	21
MnO@C nanocomposites	28	18
MnO/C nanopeapods	103	14
MnO@C microspheres	45.6	15
MnO/C microspheres	114.2	22
MnO/CNFs	79.8	19
Porous C-MnO disks	75.3	20
MnO@C nanorods	192	This work